*American Mineralogist, Volume 86, pages 124–131, 2001*

# Hydrothermal reactivity of Lu-saturated smectites: Part II. A short-range order study

**M.D. ALBA, A.I. BECERRO, M.A. CASTRO,* AND A.C. PERDIGÓN**

Departamento de Química Inorgánica. Instituto de Ciencia de Materiales, Universidad de Sevilla, Consejo Superior de Investigaciones Científicas, Avda. Américo Vespucio, 41092-Sevilla, Spain

## ABSTRACT

The short-range order of a set of Lu-saturated smectites, modified by hydrothermal treatment at 400 °C, which give rise to a new crystalline phase ($Lu_2Si_2O_7$), has been analyzed. In particular, the modifications undergone by the tetrahedral Si atoms of the lattice and the possible diffusions of O-T layer ions to other structural positions were investigated**.** Single-pulse, magic-angle-spinning nuclear magnetic resonance (MAS-NMR) measurements from the $^{1}H$, $^{7}Li$, $^{27}Al$, and $^{29}Si$ nuclei, as well as two-dimensional $^{1}H$-$^{27}Al$ cross-polarization MAS-NMR experiments, have been made on both the initial and the hydrothermally treated samples. The results show that (1) the formation of the $Lu_2Si_2O_7$ takes place from Si atoms surrounded by Al tetrahedra in the samples that contain tetrahedral Al; (2) there is a diffusion of octahedral cations to the interlayer positions during the hydrothermal treatments, compatible with the X-ray diffraction data reported for this reaction; and (3) the octahedral Al migrates to the vacant tetrahedral positions that appear during the formation of the new $Lu_2Si_2O_7$ phase. A clear relationship between each sample composition and its reactivity is defined.

## INTRODUCTION

It has been shown in Part I (Alba et al. 2001) that the reaction between the Lu ions located in the interlayer space of smectites and the Si atoms of the tetrahedral sheets to form a new crystalline phase ($Lu_2Si_2O_7$), is a general process occurring in Lu-saturated smectites treated hydrothermally at temperatures as low as 400 °C. Although the long-range order study determined the series of reactivity exhibited by the smectite family and the mineralogical properties responsible for the reactivity (i.e., the presence of tetrahedral Al and octahedral character of the mineral), that study could not elucidate several important aspects of the short-range order of the residual smectite lattice. In particular, three structural aspects discussed in Part I need to be confirmed using techniques that address short-range order. First, it was demonstrated that those minerals containing tetrahedrally substituted Al exhibit a greater reactivity for the formation of $Lu_2Si_2O_7$. Consequently, an enhanced reactivity of the Si tetrahedra surrounding these isomorphous substitutions was suggested, but no direct evidence of this fact was given. That is, no proof was provided for a greater reduction of the $Q^3(1Al)$ and $Q^3(2Al)$ Si environments than $Q^3(0Al)$ ones in samples containing both kinds of environment. [The symbology used to describe the Si environments follows the classification of Liebau (1985), where Q means a Si tetrahedron, the superscript indicates the number of corners shared with other tetrahedra, and the number of Al neighbors is specified within brackets.] Second, the noticeable amounts of $Li^+$ and $Mg^{2+}$ ions extracted from the hydrothermally treated samples led to the proposal that these ions have higher leaching rates and, consequently, occupy the interlayer positions after hydrothermal treatment. Because of the textural changes produced during the hydrothermal treatments, it was not possible to determine quantitatively the amounts of these ions that were extracted. In addition, those ions that could not be identified in the extracts obtained from the treated samples were interpreted as remaining in their previous structural locations, without any direct evidence of their actual positions. Third, a diffusion of octahedral Al ions to vacant positions in the tetrahedral sheet was suggested from DTA measurements obtained for the hydrothermally treated, Lu-exchanged Arizona montmorillonite. Again, no direct evidence was given for that migration.

In order to provide direct information on the above-mentioned structural aspects, a systematic investigation of the short-range order of the main constituents of the smectite minerals has been carried out using multinuclear solid-state nuclear magnetic resonance (MAS-NMR) spectroscopy. The following MAS-NMR experiments were performed: $^{1}H$, $^{7}Li$, $^{27}Al$, $^{29}Si$ single-pulse experiments, (SP) MAS-NMR, and two-dimensional $^{1}H$-$^{27}Al$ cross-polarization experiments, 2D $^{1}H$-$^{27}Al$ CP/MAS-NMR, on the initial and treated samples studied by Alba et al. (2001). In particular, the $^{29}Si$ (SP) MAS-NMR measurements characterize the relative abundances of the different Si environments before and after the hydrothermal treatments, directly answering the first question formulated above. Likewise, $^{1}H$ (SP) MAS-NMR can provide information on the nature of the cations present in the interlayer space of the smectites after each treatment, and the $^{7}Li$ and $^{27}Al$ (SP) MAS-NMR spectra can give direct evidence of the lattice diffusion of these ions during the hydrothermal treatment. Finally, a new method, recently developed in this laboratory (Alba et al. unpublished results), based on 2D $^{1}H$-$^{27}Al$ CP/MAS-NMR experiments, has

* E-mail: mcastro@cica.es

been applied to those samples containing structural Al, to discover the location of the octahedral Al after the hydrothermal treatments.

## EXPERIMENTAL METHODS

### Starting materials and treatments

The samples employed in this investigation are the same as those studied in our previous paper of long-range order (Alba et al. 2001): four powdered smectites (two montmorillonites, one saponite, and one hectorite) with different octahedral occupancy and tetrahedral layer charge, whose mineralogical compositions and characteristics were given in that paper. All the samples contain a content of paramagnetic ions lower than 2%. These four smectites were saturated with Lu ions and submitted to hydrothermal treatments at 400 °C for 24 hours at different water pressures, depending on the reactivity of the sample, as specified in Alba et al. (2001).

### Experimental techniques

Single-pulse experiments. (SP) MAS-NMR measurements at 9.39 T were recorded on a Bruker DRX400 spectrometer equipped with a multinuclear probe. Powdered samples were packed in 4 mm zirconia rotors and spun at 12 KHz, except for $^{7}$Li MAS-NMR measurements where the spinning rate was set at 6 KHz to study the spinning side band (SSB) structure.

$^{1}$H MAS spectra were obtained using typical $\pi/2$ pulse widths of 4.1 μs and a pulse space of 5 s. An $^{1}$H MAS spectrum from an empty rotor was collected, but no $^{1}$H background signal was recorded. Consequently, the $^{1}$H MAS spectra from samples will be shown as they were collected, without any subtraction procedure. $^{29}$Si MAS-NMR spectra were acquired at a frequency of 79.49 MHz, using a pulse width of 2.7 μs ($\pi/2$ pulse length = 7.1 μs) for all the samples. The delay time was optimized for each sample, with a strong dependence of this parameter on the Fe content of the smectite being found, as previously reported (Engelhardt and Michel 1987). The delay time employed was 3.0 s for hectorite, 2.1 s for both Arizona montmorillonite and saponite, and 1.1 s for Trancos montmorillonite. $^{27}$Al MAS-NMR spectra were recorded at 104.26 MHz for samples containing this nucleus (montmorillonites and saponite) with a pulse width of 0.92 μs ($\pi/2$ pulse length 9.25 μs) and a delay time of 0.1 s for all of them. Finally, $^{7}$Li MAS-NMR spectra at 155.51 MHz were recorded for the hectorite samples, using an optimized delay time of 1.1 s and a pulse width of 2.42 μs ($\pi/2$ pulse length =14.75 μs). The chemical shifts are reported in ppm from tetramethylsilane for $^{29}$Si and $^{1}$H, and from 0.1 *M* solutions of $AlCl_3$ and LiCl for $^{27}$Al and $^{7}$Li, respectively.

Two-dimensional $^{1}$H-$^{27}$Al cross-polarization experiments, 2D $^{1}$H-$^{27}$Al CP/MAS NMR. The technique adapted for this study is a heteronuclear, chemical-shift correlation spectroscopy (HETCOR). This technique is similar to conventional cross-polarization MAS-NMR, except that the $^{1}$H magnetization is allowed to evolve for a period $t_1$ before the magnetization is transferred to the nuclei of interest, i.e., the $^{27}$Al nuclei (Szeverenyi et al. 1982). $^{1}$H-$^{27}$Al cross-polarization experiments were performed under MAS and high-power proton decoupling using a single contact. The criteria for evaluation of a useful matching standard for quadrupolar nuclei are the same as those for spin-1/2 nuclei, except for one additional constraint: the nuclei should have a very high symmetry, the other transitions of the quadrupolar nuclei being degenerate with the central 1/2 $\leftrightarrow$ –1/2 transition (Harris and Nesbitt 1988). In this sense, a highly crystalline kaolinite was chosen as an adequate $^{27}$Al reference standard. As stated previously, this simplifies the transition contributions and essentially allows the nuclei to be treated in an analogous fashion to a spin-1/2 case. Because only the central (+1/2 $\leftrightarrow$ –1/2) transition is observed, excitation in the $^{1}$H-$^{27}$Al CP/MAS experiment is selective, and therefore the Hartmann-Hahn condition is $\gamma_H \cdot B_{1H} = 3\gamma_{Al} \cdot B_{1Al}$ and is constant for all the experiments, because both the amplifier setting and the MAS speed were kept constant. Spectra were acquired using a $^{1}$H $\pi/2$ pulse of 4.8 μs, recycle delays of 250 ms, and optimized values of contact time between 100 μs and 1 ms to detect cross peaks from a wide band of heteronuclear correlations. A 12 KHz spinning speed was chosen. A set of 80–120 FID's was obtained with a $t_1$ increment of 5 μs and a dwell time of 5 μs. The 2D Fourier transforms were calculated in absolute-value mode. A squared sine line broadening was applied in both frequency domains. The number of transients per FID and the contact time varied from spectrum to spectrum.

## RESULTS AND DISCUSSION

### $^{1}$H (SP) MAS NMR experiments

$^{1}$H MAS NMR has recently proven to be very effective in obtaining highly resolved spectra displaying distinct and well-separated signals of different types of protons in smectites (Alba et al. 2000). A typical spectrum of inorganic cation-exchanged smectites exhibits two different bands, corresponding to interlayer water molecules and structural hydroxyls, respectively. The chemical shift of the former is strongly dependent on the valence of the interlayer cations. Thus, smectites saturated with monovalent cations show a band centered at 4.1 ppm; the presence of interlayer bivalent cations shifts the signal to 4.3 ppm, and the incorporation of trivalent cations further displaces the signal to 4.6 ppm. On the other hand, the position and width of the signal associated with the structural hydroxyls are related to both the octahedral nature of the mineral and the existence of heteronuclear dipolar interactions in the sample. The hydroxyl signals at 0.65 ppm in trioctahedral smectites are narrower than those at 1.80 ppm in dioctahedral smectites. The more symmetric environment of the hydroxyl groups in the trioctahedral series, with the OH bond perpendicular to the *a-b* plane, is responsible for this effect. Finally, the presence of heteronuclear dipole-dipole interactions causes a broadening of the signals.

Figure 1 shows the $^{1}$H MAS-NMR spectra for the hydrated (left column) and dehydrated (right column) Lu-hectorite sample before (bottom lines) and after the series of hydrothermal treatments. The hydrated initial sample shows two peaks, at 4.6 and 0.4 ppm, associated with the two hydrogen environments ($H_2O$ and OH) of the structure. The dehydration of the sample causes the elimination of the 4.6 ppm water peak, as well as a slight low-field displacement and broadening of the hydroxyl peak, probably due to the closer location of the Lu interlayer cations in the dry sample. These cations in such a location can cause an electronic attraction of the hydroxyl pro-

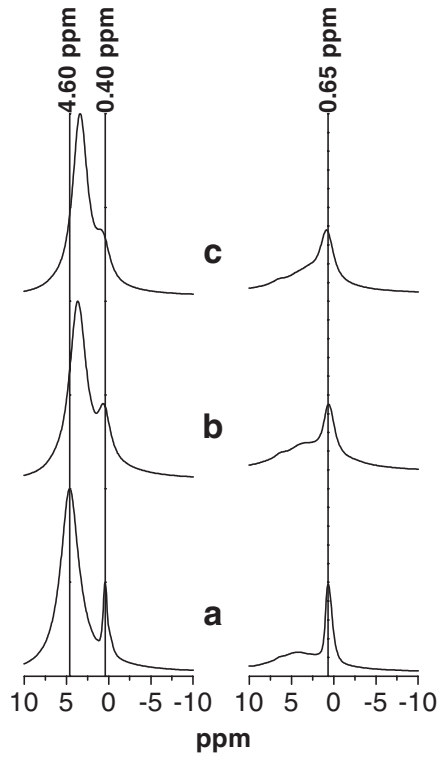


**FIGURE 1.** $^{1}$H (SP) MAS NMR spectra for the (**a**) initial and hydrothermally treated at 400 °C under a water pressure of (**b**) 200 atm and (**c**) 250 atm Lu-saturated hectorite samples equilibrated in air (left column) and after dehydration at 110 °C (right column).

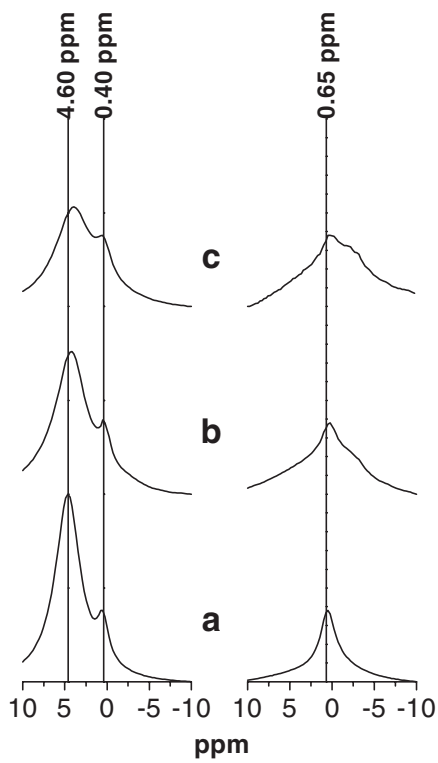


**FIGURE 2.** $^{1}$H (SP) MAS NMR spectra for the (**a**) initial and hydrothermally treated at 400 °C under a water pressure of (**b**) 150 atm and (**c**) 250 atm Lu-saturated saponite samples equilibrated in air (left column) and after dehydration at 110 °C (right column).

tons, shifting the peak to lower fields, and an increase of the heteronuclear interactions, broadening the peak. Heating at increased water pressures induces two clear changes in the $^{1}$H spectra: the water peak is shifted to a higher field, and its chemical shift after the more drastic hydrothermal treatment, at 4.1 ppm, corresponds to that due to water molecules coordinated to monovalent cations. The postulated diffusion of Li ions into the interlayer space (Alba et al. 2001) is compatible with this change. The second change observed is the broadening of the hydroxyl peak. Both the tetrahedral and octahedral vacancies created during the treatment should give rise to a more-disordered system that is compatible with this second effect.

Figure 2 displays a similar set of spectra obtained from the Lu-exchanged saponite sample. The chemical shifts of the two components are identical to those observed from the Lu-hectorite sample, in accord with the general discussion of these bands. The sole difference between them appears in the spectrum for the dry sample—the broadening shown for the hydroxyl signal in the Lu-saponite spectrum. This broadening can be interpreted in terms of both the increased heteronuclear interactions, due to more atoms with nuclear magnetic moments, and to the presence of paramagnetic impurities in that sample (Thursfield and Anderson 1996). Hydrothermal treatments again cause changes in the peakwidth of the hydroxyl signal as well as in the position of the water peak. The broadening of the hydroxyl peak again is explained as being due to the structural distortion produced in the smectite lattice during hydrothermal treatment. However, the new position observed for the water peak is not the same as that found in the hectorite sample, the maximum now being located at 4.3 ppm, compatible with an interlayer space occupied by bivalent cations. These results are in good agreement with the former discussion on diffusion of octahedral cations (Alba et al. 2001), and reinforce the idea of leaching of Mg ions in the Lu-saponite sample during the hydrothermal treatment.

Figure 3 includes the spectra for the Lu-saturated Trancos montmorillonite. The spectrum of the dry specimen shows a peak associated with the hydroxyl group at 1.8 ppm that is wider than the one observed for the saponite, in accord with the general discussion of these spectra. Unfortunately, this peak overlaps with the one due to the water molecules. Consequently, these spectra are not as useful as the former ones for elucidating the valence of the new interlayer cations, although the existence of changes similar to those observed for the other samples is clear. The Arizona montmorillonite exhibits a similar behavior and its spectra are not shown.

### $^{7}$Li (SP) MAS NMR experiments

To study the diffusion of cations from the octahedral sheet of the smectites into their interlayer space, we have recorded the $^{7}$Li MAS-NMR spectra (Fig. 4) of the hectorite sample (a smectite with $Li^{+}$ ions in the octahedral sheet) before and after

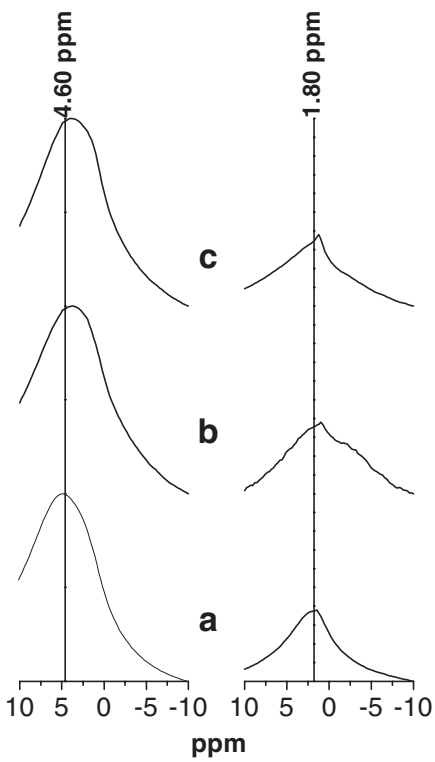


**FIGURE 3.** $^{1}$H (SP) MAS NMR spectra for the (**a**) initial and hydrothermally treated at 400 °C under a water pressure of (**b**) 150 atm and (**c**) 250 atm Lu-saturated Trancos montmorillonite samples equilibrated in air (left column) and after dehydration at 110 °C (right column).

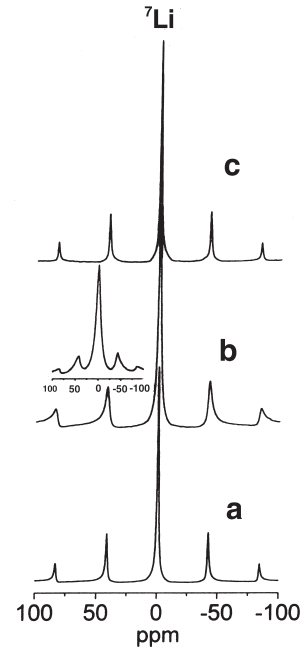


**FIGURE 4.** $^{7}$Li (SP) MAS NMR spectra of the Lu-saturated hectorite: (**a**) initial; (**b**) heated at 400 °C and 250 atm for 24 hours; and (**c**) after an ionic exchange process with Lu ions. The reduced $^{7}$Li (SP) MAS NMR spectrum included in the middle coresponds to an initial Li-saturated Trancos montmorillonite sample.

the hydrothermal treatment at 400 °C and 250 atm for 24 hours. We have also recorded the $^{7}$Li MAS-NMR spectrum of this last sample once it had been re-interchanged with $Lu^{3+}$ ions, to determine the possible removal of the interlayer $Li^{+}$ ions.

For $^{7}$Li, which has spin I = 3/2, the $m = \pm 1/2$ transition is independent of first-order quadrupolar interaction, but it is affected by second-order quadrupolar effects. In contrast with other NMR signals, variations in the coordination environment of $Li^{+}$ ions cause similar peak positions (Alba et al. 1998); however, a decrease in the electric field gradient (EFG) at the nucleus causes a decrease in the peak width as well as an increase in the sidebands intensities, due to the appearance of satellite transitions (Samoson 1985).

Despite the low Li content of the hectorite (see chemical formula in Table 1 of Alba et al. 2001), the high natural abundance of $^{7}$Li enables MAS-NMR spectra of excellent quality to be obtained without excessive demands on instrument time. The initial $^{7}$Li spectrum shows a main peak centered at –0.44 ppm with a full width at half height (FWHH) of 1.6 ppm, compatible with the data published in the literature for laponite, a synthetic hectorite (Luca et al. 1989; Bond et al. 1991; Theng et al. 1997). Four spin sidebands (SSB) can be seen in the spectra due to the lower spinning rate employed in this case. The hydrothermal treatment causes an increase of the line width in both the main signal (~3.1 ppm) and the SSB, indicating variations in the coordination environment of $Li^{+}$ that are interpreted as the partial migration of these cations from octahedral positions into the interlayer space of the hectorite. The $^{7}$Li MAS-NMR spectrum of a montmorillonite sample exchanged with $Li^{+}$ ions is shown in middle part of Figure 4. It can be seen that the spectrum of the treated hectorite is transitional between that of the untreated hectorite (with $Li^{+}$ in the octahedral sheet only) and that of a montmorillonite exchanged with $Li^{+}$ (with $Li^{+}$ in the interlayer space only), indicating the presence of this cation in both environments. The re-exchange of the hydrothermally treated hectorite with $Lu^{3+}$ ions resulted in a complete recovery of the initial spectrum, compatible with the presence of $Li^{+}$ ions in a single octahedral environment, after the ion-exchange process.

### $^{27}$Al (SP) MAS-NMR experiments

Figure 5 exhibits the $^{27}$Al (SP) MAS-NMR spectra of the initial and hydrothermally treated Arizona Lu-montmorillonite, Trancos Lu-montmorillonite, and Lu-saponite samples. The spectra obtained for the untreated samples consist of only one peak at 67 ppm for the saponite and two components centered at 0 and 67 ppm, corresponding to Al in octahedral and tetrahedral coordination, respectively (Sanz and Serratosa 1984). The asymmetry presented by the $^{VI}$Al band has been assigned by Woessner et al. (1989) to the existence of several sites of $^{27}$Al with the same coordination and similar chemical shift ($\delta$) values but different quadrupolar coupling constant (QCC) and asymmetry parameter ($\eta$) values. In the case of the Arizona montmorillonite, whose chemical formula shows a negligible content of $^{IV}$Al, the low-field peak appears at about 55 ppm, and should be assigned to a different $^{IV}$Al not belonging to the clay but to feldspar impurity, in accordance with data reported by Kirkpatrick et al. 1985.

Following hydrothermal treatment, the $^{27}$Al (SP) MAS-NMR

signals behave differently depending on the smectite. Although no changes were observed in the spectra recorded from the saponite sample, both montmorillonite spectra exhibit a progressive increase of the $^{IV}$Al peak intensity when the samples are submitted to increasing pressures. The constancy of the Al peak during the hydrothermal process in the saponite sample can be interpreted as proof of the non-diffusion of this ion from its initial location to either octahedral or interlayer environments. In contrast, the changes observed in the montmorillonite spectra indicate the diffusion of $^{VI}$Al to tetrahedral positions, probably to the tetrahedral vacancies created when the Si atoms leave their initial locations to form the new crystalline phase. This effect cannot be explained on the basis of a hypothetical redistribution of Fe ions because the same change is observed for both montmorillonites, one of them being Fe-free. However, because of the similar chemical shift presented by the $^{VI}$Al located both in the octahedral sheet and in the interlayer space, there is no evidence of a possible migration of $^{VI}$Al to the interlayer space. Such proof requires special NMR experiments, as will be shown later.

### 2D $^{1}$H-$^{27}$Al CP/MAS-NMR experiments

2D $^{1}$H-$^{27}$Al CP/MAS-NMR spectra from smectite samples have been recently obtained in our laboratory, thereby providing a new means of elucidating the different chemical environments for Al nuclei with a same coordination number (Alba et al. unpublished results). In summary, these 2D spectra allow the chemical shifts from the peaks of $^{27}$Al (SP) MAS-NMR spectra to be correlated with the proton chemical shifts from the peaks of $^{1}$H (SP) MAS-NMR spectra. Cross peaks observed in the 2D spectra indicate dipolar coupling between particular Al and proton nuclei and, therefore, determine the structural location of these Al atoms. In this study, 2D $^{1}$H-$^{27}$Al CP/MAS-NMR spectra from samples containing O-T layer Al have been recorded to obtain information on the possible diffusion of these ions through the smectite lattice during the hydrothermal treatments, one of the aims of this study.

Figure 6 includes the contour plots of the 2D $^{1}$H-$^{27}$Al correlation experiments, along with the combined 1D and 2D $^{1}$H, $^{27}$Al results, obtained from the Lu-saturated saponite before (left) and after (right) the more drastic hydrothermal treatment. The 2D spectra for each sample are shown at the top of the figure, and their 1D spectra are displayed on the axes: $^{27}$Al (SP) MAS-NMR (top) and $^{1}$H (SP) MAS-NMR (left) spectra obtained from the hydrated samples, and $^{1}$H (SP) MAS-NMR (right) spectra obtained from the samples after dehydration at 110 °C. All have been discussed in previous sections of this report. At the bottom of each contour plot, the 2D Al and proton projections are compared with the corresponding 1D MAS-NMR spectra. Both 2D spectra consist of a single cross peak, broader in the treated sample along the $^{1}$H projection. These cross peaks correlate the unique $^{27}$Al signal, corresponding to $^{IV}$Al in both cases, with the hydroxyl proton peak from the lattice. The broadening of the peak for the treated sample is compatible with the width increase observed for the hydroxyl proton 1D peak (see right 1D spectrum of this 2D contour plot). These peaks are compatible with Al ions located in the tetrahedral layer of the silicate lattice both before and after the hydrothermal treatment. The previously reported 1D $^{27}$Al (SP) MAS-NMR experiments ruled out the diffusion of Al ions from tetrahedral positions to new octahedral ones, and the 2D experiments confirm the permanence of these ions in the same O-T layer positions exhibited in the initial sample.

As regards the Al in the dioctahedral samples, a similar set of results has been included in Figure 7 for the Lu-saturated Arizona montmorillonite before and after hydrothermal treatment at 250 atm. From the results shown for the initial Lu-saturated Arizona montmorillonite, a single cross peak is again observed. However, this peak shows two differences from that for the initial Lu saponite sample: the cross peak links with the 1D $^{27}$Al octahedral signal, and this cross peak is clearly asymmetric along the horizontal axis, in accord with the original 1D

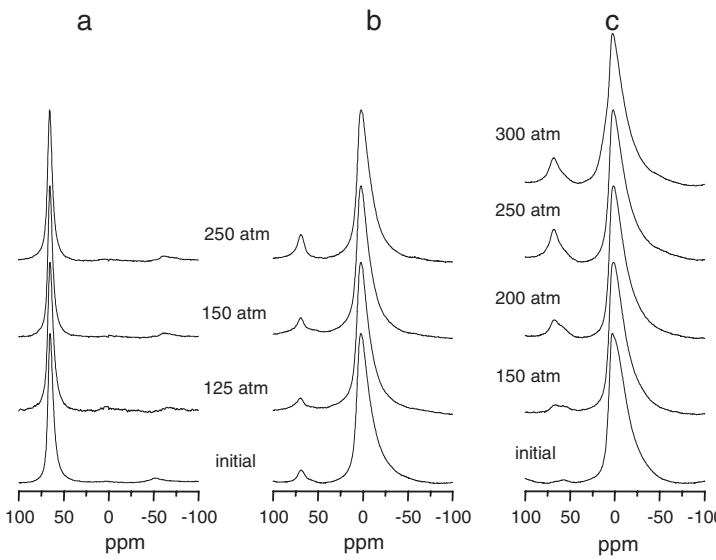


**FIGURE 5.** $^{27}$Al (SP) MAS NMR spectra of Lu-saponite (**a**), Lu-saturated Trancos montmorillonite (**b**), and Lu-saturated Arizona montmorillonite (**c**) before (initial) and after the hydrothermal treatments at 400 °C and the specified pressures.

$^{27}$Al peak. However, this cross peak links again with the 1D $^{1}$H hydroxyl peak, as in the former case. Observation of the bottom traces indicates considerable similarity between the 1D MAS NMR peaks and the corresponding 2D-projections, both for the $^{27}$Al and for the hydroxyl $^{1}$H nuclei. Thus, all the $^{27}$Al octahedral sites with different quadrupolar coupling constants and asymmetry parameters present in this sample are coupled with the hydroxyl protons of the silicate and, consequently, all of them should be located in the octahedral layer of this smectite.

The 2D contour plot following hydrothermal treatment includes only a single cross peak, linked with both the octahedral Al environment and the hydroxyl proton signal of the lattice, even when there is a tetrahedral contribution in the corresponding $^{27}$Al (SP) MAS-NMR. In this cross peak, the asymmetry shown along the horizontal line has disappeared. This difference can be observed more clearly in the bottom traces corresponding to the $^{27}$Al MAS NMR: the octahedral contribution is transformed into a more symmetrical peak, both in the 1D peak and in the 2D projection. In consequence, only certain octahedral Al ions—those appearing initially to higher field—migrate to lattice tetrahedral positions, presumably to those vacancies left by the Si atoms during the formation of

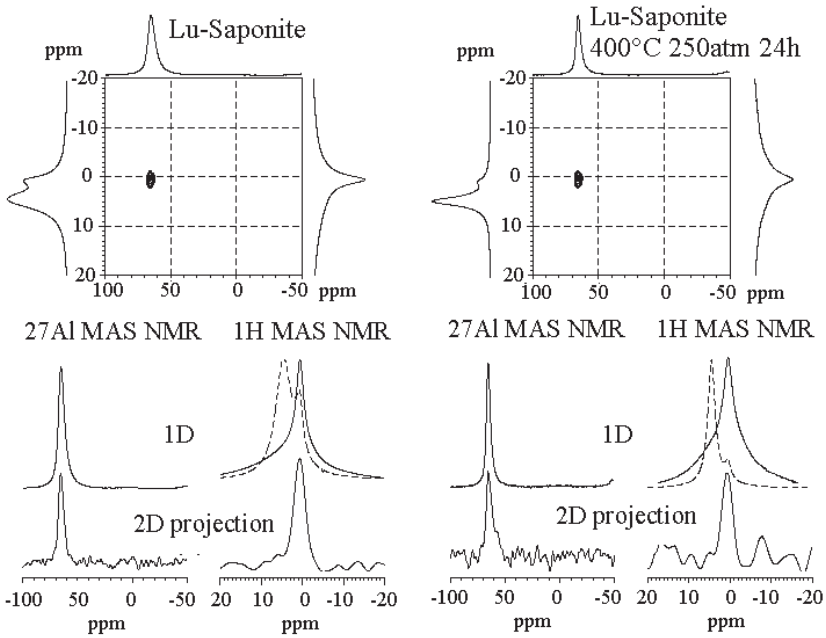


**FIGURE 6.** 2D and 1D $^{1}$H, $^{27}$Al MAS NMR spectra of the initial Lu saponite sample (left part) and that hydrothermally treated at 400 °C and 250 atm for 24 hours (right part). Upper diagrams include the contour plots of the 2D $^{1}$H-$^{27}$Al CP/MAS NMR spectra. The vertical axes represent the proton chemical-shift scales and the horizontal ones the $^{27}$Al chemical-shift scales. Lower diagrams show the single-pulse excitation 1D spectra and projections of the 2D spectra shown in the upper part for $^{27}$Al signal (left spectra) and $^{1}$H signals, in air (dashed line) and dehydrated (solid line) (right spectra).

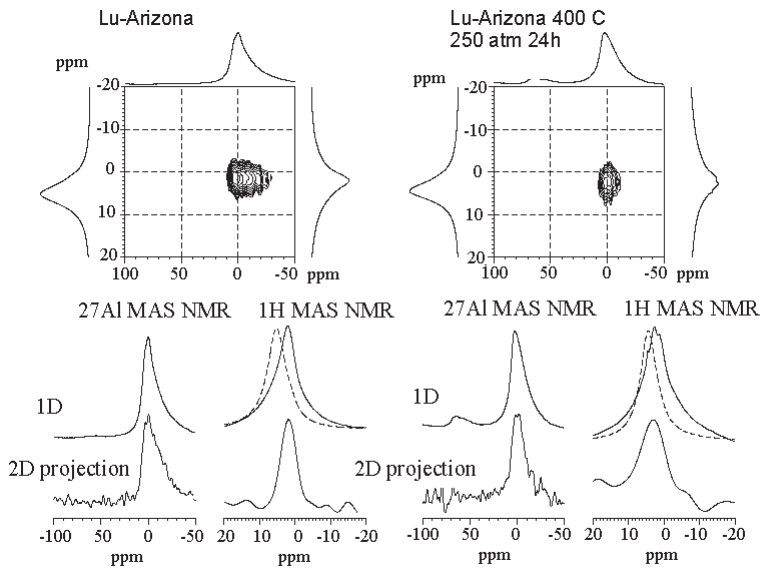


**FIGURE 7.** 2D and 1D $^{1}$H, $^{27}$Al MAS NMR spectra of the initial Lu-saturated Arizona montmorillonite sample initial (left part) and that hydrothermally treated at 400 °C and 250 atm for 24 hours (right part). Upper diagrams include the contour plots of the 2D $^{1}$H-$^{27}$Al CP/MAS NMR spectra. The vertical axes represent the proton chemical-shift scales and the horizontal ones the $^{27}$Al chemical-shift scales. Lower diagrams show the single-pulse excitation 1D spectra and projections of the 2D spectra shown in the upper part for $^{27}$Al signal (left spectra) and $^{1}$H signals, in air (dashed line) and dehydrated (solid line) (right spectra).

the new disilicate crystal. As the $^{1}H$ MAS NMR lines do not show any signal coupled with the water molecules signal, no migration to interlayer positions is inferred for this sample. The absence of a cross peak from $^{IV}Al$ could be explained by both the significantly low $^{IV}Al/^{VI}Al$ ratio and the low efficiency of the magnetization transfer between the hydroxyl protons and the tetrahedral Al atoms because of the long distance between them.

### $^{29}Si$ (SP) MAS NMR experiments

$^{29}Si$ (SP) MAS NMR spectra were recorded from the four smectites studied before and after the different hydrothermal treatments. The aim was to estimate the relative abundance of the Si signals belonging to both the smectite and the disilicate phases, as well as to investigate the formation of any other new Si signal appearing during the treatments. Representative $^{29}Si$ MAS NMR spectra are shown in Figure 8. $^{29}Si$ spectra for the initial samples are in good agreement with those expected for smectites with the formulae described in Part I and in detail elsewhere (Becerro 1997). The major component for all the samples is $Q^3(0Al)$ environments, the differences observed in their chemical shifts being a consequence of both their layer charge deficits and their octahedral nature (Sanz and Serratosa 1984). This main peak is the only one in the Arizona montmorillonite and the hectorite spectra because of the absence of $^{IV}Al$ in these structures. However, the $^{IV}Al$ content of the Trancos montmorillonite and the saponite samples causes additional Si peaks at lower fields corresponding to $Q^3(1Al)$ and $Q^3(2Al)$ environments. The integrated intensities of these contributions, calculated from theoretical Lorentzian curves, are included in Figure 9 and are in good agreement with the $^{IV}Al/Si$ ratios shown in their structural formulae.

The spectral changes of the $^{29}Si$ peaks following the different hydrothermal treatments have been monitored by integrating the intensities of the different contributions appearing in each spectrum, the same fitting procedure being used. The integrated intensities of these new spectra also have been included in Figure 9. These changes can be divided into three signal types: the new signal for $Lu_2Si_2O_7$ centered at –92.1 ppm; the main signal attributed to $Q^3(0Al)$; and those corresponding to the $Q^3(1Al)$ and $Q^3(2Al)$ environments.

The interpretation of the disilicate environment is straightforward. The signal increases for all the samples as the hydrothermal treatment is intensified, in accord with the previous XRD data. The peak areas for the disilicate Si observed for all the samples at the highest treatment are similar in all cases, and are compatible with the estimated amount of $Lu_2Si_2O_7$ for each sample, if extensive formation of the disilicate is assumed. However, the interpretation of the changes produced in the other signals is more complicated, and is related to the amount and distribution of structural Al in the lattice of the initial samples. Thus, the simplest evolution is in the Al-free sample, the hectorite. In this case, the increase in the disilicate signal is accompanied by a concomitant reduction in the $Q^3(0Al)$ peak intensity. That is, the tetrahedral Si atoms leave their initial positions to form the new crystalline phase, no more changes being observed. In the case of the Trancos montmorillonite, the $^{29}Si$ spectra of the treated samples exhibit, along with the changes mentioned above for the hectorite sample, an increase in the $Q^3(1Al)$ peak intensity, compatible with the $^{27}Al$ NMR data previously reported. A simultaneous diffusion of $^{VI}Al$ to the vacant tetrahedral positions created after the migration of the Si atoms toward the disilicate phase is, again, inferred. Spectra obtained for the saponite sample show additional changes in comparison with those for the former samples, and are more relevant to the first aim of this report—the analysis of the enhanced reactivity of the Si tetrahedra surrounded by tetrahedra containing Al atoms. Hydrothermal treatment changes the disilicate peak but causes no decrease in the $Q^3(0Al)$ peak, which remains almost constant after all the hydrothermal treatments. In turn, the integrated areas for the $Q^3(1Al)$ and $Q^3(2Al)$ environments are reduced. In this case, the disilicate phase is formed from Si atoms surrounded by one or two Al tetrahedra, the higher reactivity of these environments now being demonstrated directly.

The behavior of the Arizona montmorillonite sample is different. The appearance of the disilicate peak is accompanied by a drastic reduction in the intensity of the $Q^3(0Al)$ peak and by the appearance and growth of the peak corresponding to $Q^3(1Al)$ environments. Furthermore, a new $^{29}Si$ peak at around 108 ppm is detected in all the hydrothermally treated samples,

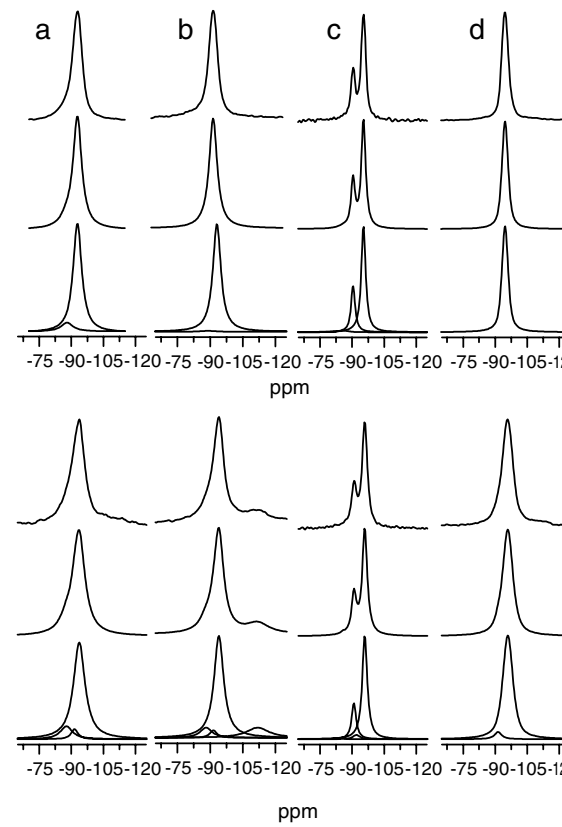


**FIGURE 8.** $^{29}Si$ MAS NMR spectra of Lu-saturated (**a**) Trancos montmorillonite, (**b**) Arizona montmorillonite, (**c**) saponite, (**d**) hectorite samples before (upper graphs) and after (lower graphs) hydrothermal treatments at 400 °C and 250 atm during 24 hours. Each graph includes the experimental spectrum (upper), the simulated one (medium), and the decomposition of simulation (lower).

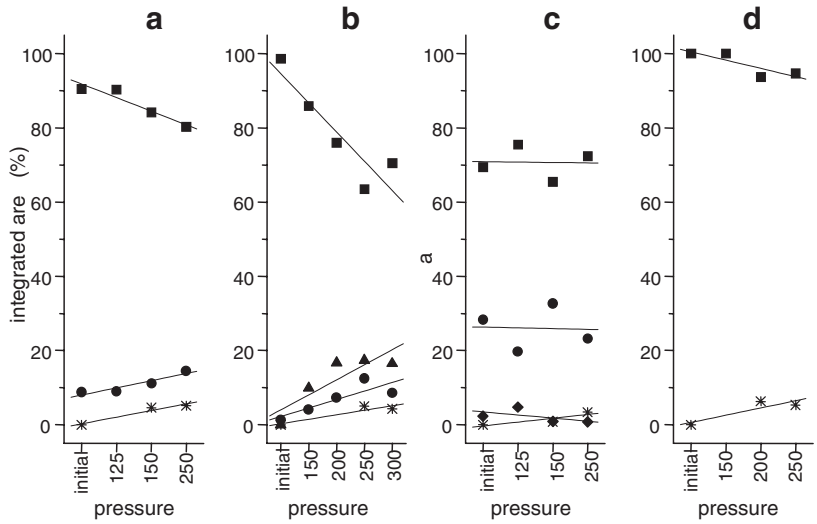


**FIGURE 9.** Integrated intensities of the different $^{29}Si$ MAS NMR signals observed in the spectra recorded from the Trancos montmorillonite (**a**), Arizona montmorillonite (**b**), saponite (**c**), and hectorite (**d**) saturated in Lu ions before and after the specified hydrothermal treatments at 400 °C. Square symbols represent $Q^3(0Al)$ environments, circles $Q^3(1Al)$, diamonds $Q^3(2Al)$, triangles $Q^4$, and stars $Q^1$.

which grows with increasing pressure. On the one hand, the increase in the intensity of the $Q^3(1Al)$ peak should be interpreted as due to the diffusion of Al ions from the octahedral to the tetrahedral sheet of the montmorillonite as observed from $^{27}Al$ NMR measurements. On the other hand, $^{29}Si$ peaks at those high fields (108 ppm) are assigned to the condensation of the Si tetrahedra forming $Q^4$ environments. Therefore, the drastic reduction in the intensity of the $Q^3(0Al)$ peak must be due to the migration of Si atoms to form both this new $Q^4$ phase and the disilicate one.

## SUMMARY

The NMR experiments reported here allow the following conclusions to be drawn. (1) $^{29}Si$ NMR experiments provide direct evidence for the different behavior of tetrahedral Si atoms during hydrothermal treatment of the smectites. In particular, the tetrahedral Si atoms located close to those occupied by Al, the $Q^3(1Al)$ and $Q^3(2Al)$ Si environments, are more reactive in forming the new $Lu_2Si_2O_7$ phase. (2) During the course of the hydrothermal treatments, cations initially located in the octahedral positions of the lattice diffuse to the interlayer space, simultaneously with the formation of the new $Lu_2Si_2O_7$ phase. In particular, $^7Li$ NMR measurements indicate the migration of these nuclei as well as the exchangeability of these ions with other cations contained in a solution in contact with the smectite. $^{27}Al$ NMR spectra demonstrate that these ions do not migrate to interlayer positions after hydrothermal treatment, which is compatible with the lower reactivity shown by the dioctahedral samples and with the leaching rate reported for this ion in the literature. (3) Octahedral Al ions migrate to vacant tetrahedral positions during the hydrothermal treatments, filling the tetrahedral vacancies created after the migration of Si atoms that formed the $Lu_2Si_2O_7$ phase. Such migration alters the tetrahedral composition of the smectite lattice, and may induce changes in the further reactivity of the samples.

## ACKNOWLEDGMENTS

The Spanish DGICYT is thanked for financial support (Project no. PB97-0715), and A.I.B. thanks the Spanish M.E.C. for a predoctoral fellowship which allowed carrying out the experimental work included in this report.

## REFERENCES CITED

Alba, M.D., Alvero, R., Becerro, A.I., Castro, M.A., and Trillo, J.M. (1998). Chemical Behavior of Lithium Ions in Reexpanded Li-Monrtmorillonites. Journal of Physical Chemistry B 102, 2207–2213.

Alba, M.D., Becerro, A.I., Castro, M.A., and Perdigón, A.C. (2000) High-resolution $^1H$ MAS NMR spectra of Phyllosilicates 2:1. Journal of the Chemical Society. Chemical Communications, 37–38.

Alba, M.D., Becerro, A.I., Castro, M.A., and Perdigón, A.C. (2001) Hydrothermal reactivity of Lu-saturated smectites: Part I. A long-range order study. American Mineralogist, 86, 115–123.

Becerro, A.I. (1997) Desarrollo de un sistema modelo de análisis estructural de la reactividad química de compuestos de silicio 2D y 3D aplicado a la formación de $Lu_2Si_2O_7$, Ph.D. dissertation. Universtiy of Seville, Seville.

Bond, S.P., Gelder, A., Homer, J., McWhinnie, W.R. and Perry, M.C. (1991) $^6Li$ Magic Angle Spinning Nuclear Magnetic Resonance Spectroscopy: A Powerful Probe for the Study of Lithium-containing Materials. Journal of Materials Chemistry, 1, 327–330.

Engelhardt, G. and Michel, D. (1987) High Resolution Solid State NMR of Silicates and Zeolites. Wiley, New York.

Harris, R.K. and Nesbitt, G.J. (1988) Cross Polarization for Quadrupolar Nuclei—Proton to Sodium-23. Journal of Magnetic Resonance, 78, 245–256.

Kirkpatrick, R.J., Kinsey, R.A., Smith, K.A., Henderson, D.M., and Oldfield, E. (1985) High-resolution solid-state Na-23, Al-27, and Si-29 nuclear magnetic-resonance spectroscopic reconnaissance of alkali and plagioclase feldspars. American Mineralogist 70, 106–123.

Liebau, F. (1985) Structural chemistry of silicates. Springer-Velag, Berlin.

Luca, V., Cardile, C.M., and Meinhold, R.H. (1989) High-Resolution Multinuclear NMR Study of Cation Migration in Montmorillonite. Clay Minerals, 24, 115–119.

Samoson, A. (1985). Satellite Transitions High-Resolution NMR of Quadrupolar Nuclei in Powders. Chemical Physics Letters, 119, 29–32

Sanz, J. and Serratosa, J.M. (1984) $^{29}Si$ and $^{27}Al$ High-Resolution MAS-NMR Spectra of Phyllosilicates. Journal of the American Chemical Society, 106, 4790–4793.

Szeverenyi, N.M., Sullivan, M.J., and Maviel, G.E. (1982) Observation of Spin Exchange by Two-Dimensional Fourier Transform $^{13}C$ Cross Polarization-Magic-Angle Spinning. Journal of Magnetic Resonance, 47, 462–475.

Thursfield, A. and Anderson, M.W. (1996) $^1H$, $^2H$ and $^{13}C$ Solid-State NMR studies of methanol adsorbed on a series of acidic microporous zeotype materials. Journal of Physical Chemistry, 100, 6698–6707.

Theng, B.K.G., Hayashi, S., Soma, M., and Seyama, H. (1997) Nuclear Magnetic Resonance and X-ray Photoelectron Spectroscopic Investigation of Lithium Migration in Montmorillonite. Clays and Clay Minerals, 45, 718–723.

Woessner, D.E. (1989) Characterization of clay minerals by $^{27}Al$ nuclear magnetic resonance spectroscopy. American Mineralogist, 74, 203–215.

MANUSCRIPT RECEIVED JUNE 18, 1999
MANUSCRIPT ACCEPTED SEPTEMBER 3, 2000
PAPER HANDLED BY MARK WELCH